Membrane curvature association of amphipathic helix 8 drives constitutive GPCR endocytosis

Rasmus Herlo*[1], Jan Hendrik Schmidt*[1], Joscha Rombach[1], Andreas Haahr Larsen[1], Mikkel Stoklund[1], Mathias Perslev[1], Tommas Theiss Ehlers Nielsen[1], Keenie Ayla Andersen[1], Carmen Klein Herenbrink[1], Matthew D. Lycas[1], Aske Lykke Ejdrup[1], Nikolaj Riis Christensen[1], Jan P. Christensen[2], Mootaz Salman[3], Freja Herborg[1], Ulrik Gether[1], Alexander Sebastian Hauser[4], Patricia Bassereau[5], David Perrais[6], Kenneth Lindegaard Madsen[1]

[1]Molecular Neuropharmacology and Genetics Laboratory, Department of Neuroscience, Faculty of Health and Medical Sciences; University of Copenhagen, 2200 Copenhagen N, Denmark.

[2]Department of Immunology and Microbiology, Faculty of Health and Medical Sciences; University of Copenhagen, 2200 Copenhagen N, Denmark.

[3]Department of Physiology, Anatomy and Genetics, Wolfson College, University of Oxford, Oxford OX1 3QU, UK

[4]Department of Drug Design and Pharmacology, University of Copenhagen, 2100 Copenhagen, Denmark

[5]Institut Curie, Université PSL, Sorbonne Université, CNRS UMR168, Laboratoire Physico-Chimie Curie, 75005 Paris, France

[6]Univ. Bordeaux, CNRS, Interdisciplinary Institute for Neuroscience; IINS, UMR 5297, 33000 Bordeaux, France.

*These authors contributed equally to this work

Correspondance: kennethma@sund.ku.dk

One-Sentence Summary

Receptor proteins navigate cellular membranes by interacting with their curvature using an evolutionary conserved mechanism that complements direct coupling to the endocytic protein machinery.

Abstract

Cellular signalling relies on the activity of transmembrane receptors and their presentation on the cellular surface. Their continuous insertion in the plasma membrane is balanced by constitutive and activity dependent internalization, which is orchestrated by adaptor proteins recognizing semi-specific motifs within the receptors' intracellular regions. Using multiple of fluorescence-based cellular assays, we discover a complementary and evolutionary conserved trafficking mechanism for G-protein coupled receptors, which relies on the insertion of their amphipathic helix 8 (H8) into the inner leaflet of lipid membranes, orthogonal to the transmembrane helices. These amphipathic helices autonomously drive endocytosis of receptors by cooperative assembly and association with areas of high membrane curvature. The strength of H8 membrane insertion propensity quantitatively predicts the rate of constitutive internalization of G-proteins coupled receptors.

Introduction

Cellular trafficking and sorting processes direct transmembrane proteins (TMPs) to their proper destination within the cell. Consequently, these processes are of fundamental importance for cellular homeostasis, metabolism, and communication. Malfunction results in diseases including

21 cancer, metabolic syndroms, neuropathies, neuro-degenerative disease and psychiatric
22 disorders [1].

23 Vesicular membrane carriers are responsible for the transport of TMPs between different
24 cellular compartments and TMP cargo selection is typically mediated by semi-specific protein-
25 protein interactions between compartment specific adaptor proteins (e.g. AP1-5 and GGAs) and
26 short linear motifs within the cargo TMPs (e.g. FXNPXY, tyrosine- and dileucine-based signals) [2,3].
27 The initial budding and formation of these carriers involve generation of high membrane
28 curvature which serves to recruit specific scaffolding and regulatory cytosolic proteins [4,5]. This
29 mechanism, termed membrane curvature sensing (MCS), is commonly mediated by
30 amphipathic helices (AHs) that insert partially into exposed lipid packing defects in the convex
31 leaflet of curved membranes [6,7]. We hypothesized that AH motifs located in the intracellular
32 termini of TMPs, positioned at the membrane-cytoplasm interface, serve to partition TMPs into
33 areas of high curvature during formation of vesicular carriers. Using G protein-coupled receptors
34 (GPCRs) as example, our data demonstrates that AHs direct constitutive trafficking of TMPs with
35 rates quantitatively predicted by their membrane insertion propensity (MIP). We demonstrate
36 that this new trafficking mechanism for TMPs, relying on their direct association with highly
37 curved membranes in budding membrane carriers, is fundamentally distinct from conventional
38 adaptor-based TMP trafficking processes, such as that underlying agonist-induced
39 internalization. Moreover, we present data suggesting that it is evolutionary conserved across
40 GPCR families and animal species. We refer to this mechanism as Trafficking of Transmembrane
41 proteins by Amphipathic Motifs (ToTAM).

42 # Results

43 ## Amphipathic helices drive constitutive internalization of transmembrane proteins

44 G protein-coupled receptors (GPCRs) constitute the largest family of TMPs in the human
45 genome, they control vital physiological functions, and represent targets for roughly a third of
46 all approved drugs [8]. GPCRs consist of 7 transmembrane α-helices and an amphipathic 8th helix
47 (H8) that can insert into the cytosolic leaflet of the membrane orthogonal to the
48 transmembrane helices (Figure 1A) [9–12]). Interactions between H8 and cytosolic adaptor proteins
49 are known to mediate various trafficking processes, particularly agonist-induced endocytosis,
50 but also constitutive internalization [13]. We tested a putative autonomous function of H8 in
51 endocytosis in a membrane-anchored context, by fusing peptide sequences harboring H8 (17-18
52 residues) from a number of well-characterized class A GPCRs (rhodopsin (Rho), β2 adrenergic
53 receptor (β2), substance P receptor (NK1)), and dopamine D2 receptor (D2) to the cytosolic C-
54 terminus of the internalization inert transmembrane interleukin-2 receptor a-subunit (IL-2a),
55 hereafter referred to as Tac (Figure 1A) [14,15].

56 The fusion of AHs increased internalization of Tac as determined by quantitative confocal
57 microscopy of antibody feeding experiments in HEK293 cells (up to 10-fold for Tac-D2) (Figure
58 1B-C). Disrupting the hydrophobic wedge of the amphipathic helices by introducing negative
59 charges (Figure 1A) abrogated this effect (Figure 1B-C). We recapitulated these findings in HeLa
60 cells (Figure S1). Alanine substitution of cysteines, previously shown to modify trafficking of
61 GPCRs through acylation [16], did not compromise internalization (Figure S2).

After confirming the relative internalization rates with high-throughput quantitative flow cytometry [17] (Figure S3), we showed that five additional H8s with distinct amphipathic nature, i.e., with high hydrophobic moment, also increased Tac internalization (Figure 1D). These were H8 from trace amine receptor 1 and 6 (TA1 and TA6), □ opioid receptor (□), dopamine D1 receptor (D1) and angiotensin 2 type 1 receptor (AT1) (biochemical parameters outlined in Figure S4). To consolidate and broaden these findings, we also tested non-GPCR helices. Fusion of a hydrophilic helix from troponin [18] or the hydrophobic helix from citrate [19] did not increase Tac internalization, whereas AHs of several membrane-associated proteins involved in membrane trafficking, including Amphipathic Lipid Packing Sensor (ALPS), Sar1 and Endophilin A1, but not Epsin-1 [20,21] facilitated internalization (Figure 1E). Similarly, exogenous AHs, including the bee venom Melittin, the bacterial protein SpoVM and the artificial AH Hecate, strongly facilitated internalization. Together these findings demonstrate that AHs, diverse in origin and devoid of known adaptor motifs, autonomously increase endocytosis of a transmembrane protein. We define this mechanism as Trafficking of Transmembrane proteins by Amphipathic Motifs (ToTAM).

To quantify the propensity of the individual AHs to associate with positive membrane curvature, we adjusted the calculated hydrophobic moment of AHs by their intrinsic helical propensity (see methods) [22]. The resulting value, membrane insertion propensity (MIP), correlated with empirical measures of membrane association strength as determined by liposome binding to peptides on a SPOT array (Figure S5). Furthermore, plotting internalization of the AH-fused Tac-constructs as a function of MIP yielded a remarkably strong correlation irrespective of the origin of the AHs (Figure 1F), demonstrating that AHs drive internalization of TMPs in a highly

84 predictive manner. Comparatively, net charge and hydrophobicity demonstrated less predictive
85 power on their own (Figure S6). In absolute terms, introduction of AHs increased internalization
86 from a basal level of 20% of Tac over a 30-minute period to a complete (100%) turnover of Tac-
87 AHs for the strongest AHs (Figure S7).

88 Finally, to address the endocytic function of H8 in context of full-length receptors, we focused
89 on β2 and AT1, that contain H8s with pronounced differences in their autonomous endocytic
90 drive (Figure 1F). In concordance, AT1 displayed significantly higher constitutive internalization
91 than β2, and this pattern was reversed by swapping their helices (Figure 1G-H and S8).
92 Furthermore, the introduction of the potent AH Hecate gave rise to an even higher
93 internalization rate than that of AT1. In contrast, internalization in presence of agonist was
94 robust for all constructs irrespective of AH (Figure 1H and S8). Further, while constitutive
95 internalization scaled linearly with expression, agonist induced internalization for the H8
96 containing constructs deviated from linearity consistent with saturation of adaptor-based
97 internalization machinery (Figure S8). This suggests that MIP of H8 drives constitutive, but not
98 agonist-induced, internalization of GPCRs in a mechanistically novel fashion.

99 AH driven Internalization is temporally dissociated from CME

100 Next, we chose a series of five Tac-AHs, spanning from low to high MIP values and assessed
101 their differential association with endocytic machineries using a proximity biotinylation
102 approach followed by quantitative label-free LC-MS² (Figure 2A) [23]. Importantly, the BioID2-
103 fusion constructs recapitulated ToTAM driven internalization (Figure 2B and S9A-B). The Tac-AHs
104 conferred low enrichment of biotinylated cytosolic proteins relative to control cells not

105 expressing the BioID2 construct, whereas labeling of plasma membrane proteins was strongly
106 enriched (Figure 2C and S9E). This enrichment of plasma membrane proteins was gradually
107 reduced with increasing MIP of the residing AHs, consistent with an increased internalization
108 and/or reduced maturation of these constructs (Figure 2D).

109 The MIP of the expressed Tac-AHs did not significantly affect the enrichment of actin, (Figure 2C
110 and S9F) consistent with a reduced impact of treatment with the actin polymerization inhibitor
111 Latrunculin A on internalization of Tac-AHs with high MIP (Figure S10A-C). Dynamin showed
112 slight enrichment with increasing MIP of the AHs and all constructs showed reduced
113 internalization upon Dyngo-4A treatment, indicating at least a partial dependence on dynamin
114 (Figure S10A-C). Likewise, ATP-depletion reduced internalization for all constructs albeit
115 relatively less for Tac-AHs with high MIP (Figure S10D-F).

116 Overall, key proteins of clathrin-mediated endocytosis (CME)[24], and in particular clathrin and
117 EPS15, were enriched for all AHs. On the other hand, identified components of the GLIC/GEEC
118 pathway, as well as caveolae[25,26], were consistently less enriched with increasing MIP of the AHs
119 (Figure 2E). Finally, enrichment of proteins involved in alternative endocytic pathways, including
120 Arf6, Rac1, Endophilin A2, and Flotillins (FLOT1 and FLOT2 [27]), were relatively independent of
121 MIP. Grouping all identified CME associated proteins according to temporally defined modules
122 [28], we observed no marked increase in association with nucleation and assembly, neck
123 constriction or scission and movement modules, while proteins involved in uncoating as well as
124 endosome fusion were enriched for all AHs (Figure S9G). Notably, proteins of the nucleation and
125 formation module that showed an increased abundance, including clathrin and EPS15,
126 represented a group that has been shown to be continuously associated with CME events until

127 uncoating [24]. Together, this could indicate that ToTAM may accelerate maturation of CME
128 structures or substitute for several of the proteins involved in maturation, including, e.g., BAR
129 domain proteins (Figure S9H). EPS15 is known to recruit ubiquitinated cargo to endocytic sites
130 [29]. In accordance, we detected minor increases in ubiquitin binding proteins of the ESCRT
131 machinery and E3 ubiquitin ligases [30], however, this could simply reflect the localization of these
132 components to intracellular membranes (Figure S9I-J). Taken together, ToTAM associates with
133 CME rather than GLIC/GEEC pathway, caveolae or alternative pathways, and displays a MIP
134 dependent association with dynamin. Notably, we found no association between Tac-AHs and
135 any classical or putative novel adapter proteins.

136 To directly evaluate the trafficking dynamics of Tac-AH constructs and the CME structures they
137 associate with, we turned to pulsed pH (ppH) TIRFM assay [31] using super ecliptic pHluorin (SEP)
138 tagged constructs co-expressed with mCherry-tagged clathrin light chain (CLC) (Figure 2G-H and
139 S11). Corroborating the biochemical findings, the number of endocytic events increased by
140 almost an order of magnitude with increased MIP of the AHs, approaching the rate of the
141 transferrin receptor (TfR) for the strongest helices (H8 from AT1, and Hecate) (Figure 2I).
142 Interestingly, exocytosis increased correspondingly, suggesting efficient intracellular sorting to
143 recycling endosomes (Figure S12). CLC fluorescence intensity traces associated with TfR
144 endocytic events displayed a typical profile with gradual accumulation until point of scission
145 followed by a rapid decrease after scission (Figure 2J). This distinct profile was gradually lost
146 with increasing MIP of the Tac-AH constructs indicating desynchronization with the CME
147 machinery. Individual normalized traces displayed a range of CLC recruitment profiles (Figure
148 S13). Principal component analysis (PCA) revealed a decreasing fraction of traces similar to the

149 typical TfR-associated CLC profile for Tac-AHs with increasing MIP (Figure S14). Conversely, an
150 increased fraction of events displayed accumulation of CLC immediate post scission. In
151 summary, increased MIP directs ToTAM towards bulk association with CME core machinery at
152 the cost of other endocytic machineries, while simultaneously decreasing the temporal
153 synchronization and coordination with clathrin-dynamics.

154 Membrane curvature association facilitates internalization

155 Next, we analyzed the recruitment dynamics of the SEP-Tac-AH constructs prior to scission
156 (Figure 3A). While TfR accumulates slowly during vesicle formation [32], the AH-linked profiles
157 showed accelerating kinetics with increasing MIP of AHs. Fitting these profiles with a logistic
158 equation showed increasingly cooperative clustering mechanism consistent with an auto-
159 nucleating function (Figure 3B). This effect implies an increased rate of maturation of endocytic
160 structures, which was supported by the observed MIP dependent effect on Tf-uptake in trans
161 (Figure 3C). Taken together, we find that ToTAM is characterized by numerous, fast and
162 cooperative endocytic events with the potential to accelerate overall trafficking rates.

163 The desynchronization with canonical endocytic machinery, the cooperative recruitment and
164 the inductive properties together indicate an underlying autonomous and recursive mechanism,
165 resulting from concurrent membrane curvature sensing and induction, a common characteristic
166 of AH association with lipid membranes. We therefore investigated the MCS properties of
167 Hecate (the AH with highest tested MIP) in a buckled membrane system using molecular
168 dynamics simulation. This simulation predicted a curvature sensitive membrane sorting (Figure
169 3D-E), akin to ALPS [33]. We experimentally confirmed this finding by pulling tethers from a GUV

170 preincubated with OG488-Hecate, observing a significant enrichment in areas of high curvature
171 (peptide on tether relative to GUV) (Figure 3F-G). Reducing helical propensity and MIP of the
172 helix, while keeping charge constant, disrupted binding to GUVs (Figure S15A-B). Consistent
173 with the cooperative clustering observed in the ppH-TIRF experiments, the Hecate peptide
174 occasionally formed microdomains on GUVs in the absence of manipulation (Figure S15C).

175 To assess the size and curvature of the endocytic budding structures prior to scission, we
176 antibody-labelled surface expressed Tac-AHs for 3D-dSTORM imaging and identified protein
177 clusters using DBSCAN analysis (Figure 3H and S16). While the median radius of clusters was 100
178 nm for Tac, consistent with the size of clathrin-coated pits (CCPs), cluster sizes were consistently
179 smaller with increasing MIP of AHs (Figure 3I). In accordance, cargo load of pH 5.5 events at
180 point of scission in ppH-TIRFM experiments was decreased with increasing MIP of AHs (Figure
181 S17). Protein densities of individual budding structures obtained by 3D-dSTORM gradually
182 approached a linear dependence on size with increasing MIP of the AHs (Figure 3J-K), as
183 previously modelled for insertion-based membrane curvature sensing [6]. Estimates from relative
184 protein density and quenching rates of vesicular carriers immediately post-scission obtained
185 from ppH-TIRFM experiments supported increased protein density in endocytic structures
186 containing Tac-AHs with high MIP (Figure S17). In summary, we propose that ToTAM
187 mechanistically serves both to localize cargo to endocytic pits as well as to facilitate the
188 membrane curvature induction and possibly scission of these pits to drive endocytosis.

189 ## Membrane insertion propensity is evolutionary conserved across distant organisms

190 Next, given the conservation of amphipathic periodicity in H8 across GPCR families [34] (Figure
191 S18A), we upscaled the liposome binding SPOT assay (Figure S5) to a large-scale chip array
192 format (Figure 4A-B). This allowed us to scan through the full range of human GPCR C-termini,
193 without compromising assay performance (Figure S18B). Binding profiles demonstrated a
194 confined membrane binding region overlapping with the H8 region (consecutive high MIP-
195 values) as illustrated by the C-terminal regions of rhodopsin, β2 and AT1 (Figure 4C). Averaged
196 membrane binding for each of the GPCR families confirmed this pattern for rhodopsin
197 (disregarding olfactory receptors), secretin and frizzled families, albeit with membrane binding
198 extending slightly further away from the TM region for the latter. Membrane binding was less
199 pronounced for the remaining families and absent from the glutamate receptor family (Figure
200 S18C). UMAP analysis of the binding profiles revealed a group of GPCRs (cluster 1) without
201 membrane binding, while clusters 2-5 showed membrane binding profiles consistent with
202 membrane proximal H8, albeit with increasing length and distance from TM7 from cluster 2 to 5
203 (Figure 4D-E and Figure S19). In contrast, cluster 6 contained a wide range of different
204 membrane binding profiles, which are distant from TM7 and/or contain multiple membrane
205 binding sites. We did not observe an enrichment of individual clusters within GPCR receptor
206 families (Figure S18D), specific tissues (Figure S18E) or Gene Ontology (GO) terms (data not
207 shown).

208 The experimentally derived membrane binding profiles enabled us to calculate MIP values for
209 the regions corresponding to bona fide H8s (clusters 2-5, Figure S20), while the lack of
210 membrane binding in cluster 1, precluded calculation of MIP values. We previously

211 characterized the constitutive internalization of a range of pharmacologically relevant GPCRs [35]
212 and here asked if this internalization could be explained by MIP values of the regions defined by
213 their membrane binding profiles. Constitutive internalization significantly correlated with MIP
214 (cluster 2-5) (Figure 4F), however, traditional biophysical measures, alternative to MIP, failed to
215 explain constitutive internalization (Figure S21A-C). The complex membrane binding profiles
216 cluster 6 precluded extraction of MIP values predictive of constitutive internalization (Figure
217 S21D). Consistent with the lack of effects of H8 substitution on agonist induced internalization
218 (Figure 1H), MIP did not correlate with agonist-induced internalization (Figure S21E). Together,
219 these results indicate that the MIP of H8 selectively predicts constitutive internalization across
220 this functionally important and structurally well-characterized subset of GPCRs.

221 Given the functional importance of constitutive internalization for dynamic surface expression
222 of GPCRs, we utilized MIP for H8 as a proxy to map predicted internalization rates across all non-
223 odorant GPCRs belonging to cluster 2-5 (Figure 4G and S21F). High MIP values are
224 predominantly observed as phylogenetically related clusters within the rhodopsin family of
225 receptors, including receptors for biogenic amines, chemokine receptors, and MAS-related
226 receptors as well as free fatty acid receptors and individual receptors such as NPBW2 and
227 C5AR1. We also note that Secretin and Frizzled receptors largely contained a H8 predicted or
228 found to be longer than 20 residues and the functional significance of this remains to be
229 explored. Notably, MIP is not significantly related to β-arrestin recruitment and reported G-
230 protein coupling (Figure S22A-B).

231 To assess functional conservation of high MIP of H8, we used data from UK biobank on naturally
232 occurring variants in human GPCRs. While the cost of individual amino acid substitutions was

233 similar, the frequency of non-synonymous natural variants was significantly lower within H8s
234 compared to the remaining C-terminus (Figure S23A-B). Moreover, the observed natural
235 variants give rise to more conserved MIP than potential substitutions not observed (Figure
236 S23C). Finally, the frequency of natural variants within H8 for individual receptors declines with
237 increasing MIP, emphasizing the functional conservation of high MIP (Figure S23D). This
238 functional selection is further evident from the multimodal distribution of H8 MIP values across
239 human GPCRs, significantly different from a normal distribution (Figure 4H, $p < 0.0001$, Shapiro-
240 Wilk). Sub-groups of GPCRs shown to be directed to the Fast Endophilin-Mediated Endocytosis
241 (FEME) pathway, to mediate endosomal signaling or to function as mechanosensitive GPCRs
242 display H8 MIP value distributions similar to this overall distribution. GPCRs associated with
243 primary cilia, which exhibit inverse curvature topology to endocytic structures, on the other
244 hand, display H8 sequences with significantly lower MIPs. Conversely, GPCRs expressed by
245 viruses, which are known to elicit high constitutive internalization [36], mostly have high MIP
246 values of their H8 (Figure 4H and S22C).

247 GPCR C-termini from evolutionary distant organisms, including C. elegans, D. Melanogaster and
248 S. Cerevisiae, show membrane binding profiles akin to H8 in human GPCRs (cluster 2 and 3) as
249 well as non-binding (cluster 1) and more complex binding profiles (cluster 4 and 5) (Figure S24).
250 This enabled us to address evolutionary conservation across species by aligning H8 sequences
251 defined in human across species back to Ecdysozoa (Figure 4H). Individual receptors show
252 strong conservation of MIP throughout evolution, and the relative variation across species is
253 lowest for H8s with high MIP (Figure 4H, top). Additionally, the fraction of receptors with high
254 MIP of H8 (> 0.3) gradually increase in higher organisms indicating functional significance

255 (Figure 4H). Together, this demonstrates both evolutionary selection and functional
256 conservation of H8 in GPCRs with high MIP.

257 Discussion

258 Here we show that AHs enable TMPs to associate with areas of high membrane curvature
259 similar to what has been demonstrated for cytosolic proteins. For TMPs, this association
260 accelerates their constitutive trafficking in a manner that correlates with the MIP of the AH.
261 While this paper has exclusively addressed endocytosis and recycling, we hypothesize that this
262 mechanism, due to the basic biophysical principle, will generalize to trafficking events
263 throughout the endomembrane system involving highly curved membrane topologies. We term
264 this mechanism ToTAM.

265 Mechanistically, ToTAM is characterized by fast, cooperative cargo recruitment into small,
266 spherical, high-density carriers and thus ToTAM displays elements of both membrane curvature
267 sensing and facilitation of the cargo/carrier complex formation. In fact, ToTAM increases
268 endocytosis of the transferrin receptor in trans, implying an active impact on endocytic
269 processes. During this process, partial biochemical association with CME was observed,
270 however, actual CLC accumulation prior to scission was low and increasingly asynchronous with
271 higher MIP. Together, our data suggest that ToTAM might hijack nucleation involving CLC and
272 EPS15 to shortcut classical CME in a relatively autonomous fashion that is complementary to
273 the established adaptor based endocytic machinery.

274 This specific impact of high MIP H8 on constitutive, and not agonist-induced, internalization of
275 full length GPCRs, was causally demonstrated by experiments with chimeric receptors. Using

276 large-scale liposome-binding data to exclude GPCRs with C-termini that did not display
277 membrane-binding or complex membrane binding enabled us to correlate H8 MIP with full-
278 length constitutive internalization across all human GPCRs. Highest constitutive internalization
279 was bioinformatically predicted for the groups of chemokine receptors, biogenic amine
280 receptors, MAS-related receptors, and free fatty acid receptors. It will be interesting to elucidate
281 the functional implication of the predicted high constitutive turnover with e.g. ligand
282 scavenging, membrane modulating ligands or continuous receptor availability.

283 Another recently described membrane-associated function of H8 is its role in conferring
284 mechanosensitivity to GPCRs [37]. Several of these receptors include a H8 with high MIP, including
285 H1, AT1, and S1P1, and a putative interplay between mechanosensation and high constitutive
286 internalization due to membrane curvature sensing might reflect two aspects of the same
287 biophysical principle and functional implications of these might unveil themselves perhaps in
288 the context of the cardiovascular system. Moreover, GPCRs implicated in viral entry, as well as
289 virally expressed GPCRs displaying high constitutive internalization, all except mGluR2 show high
290 MIP [38], potentially advocating a novel molecular target for anti-viral therapy. Finally, the simple
291 molecular nature of ToTAM is compatible with an early evolutionary origin, dating back prior to
292 the yeast GPCRs characterized here, conceivably even prior to adaptor based trafficking.
293 Ultimately, functional studies will be needed to settle the evolutionary relation between these
294 two complementary trafficking mechanisms.

295 ## References
296

1. McMahon, H. T. & Boucrot, E. Molecular mechanism and physiological functions of clathrin-mediated endocytosis. *Nature Reviews Molecular Cell Biology* vol. 12 517–533 Preprint at https://doi.org/10.1038/nrm3151 (2011).

2. Bonifacino, J. S. & Traub, L. M. Signals for sorting of transmembrane proteins to endosomes and lysosomes. *Annual Review of Biochemistry* vol. 72 395–447 Preprint at https://doi.org/10.1146/annurev.biochem.72.121801.161800 (2003).

3. Sanger, A., Hirst, J., Davies, A. K. & Robinson, M. S. Adaptor protein complexes and disease at a glance. *J Cell Sci* **132**, (2019).

4. McMahon, H. T. & Boucrot, E. Membrane curvature at a glance. *J Cell Sci* **128**, 1065–1070 (2015).

5. Antonny, B. Mechanisms of Membrane Curvature Sensing. *Annu Rev Biochem* **80**, 101–123 (2011).

6. Hatzakis, N. S. *et al.* How curved membranes recruit amphipathic helices and protein anchoring motifs. *Nat Chem Biol* **5**, 835–841 (2009).

7. Drin, G. & Antonny, B. Amphipathic helices and membrane curvature. *FEBS Lett* **584**, 1840–1847 (2010).

8. Hauser, A. S., Attwood, M. M., Rask-Andersen, M., Schiöth, H. B. & Gloriam, D. E. Trends in GPCR drug discovery: New agents, targets and indications. *Nat Rev Drug Discov* **16**, 829–842 (2017).

9. Palczewski, K. *et al.* Crystal Structure of Rhodopsin : A G Protein – Coupled Receptor. **289**, 739–746 (2000).

10. Isberg, V. *et al.* GPCRdb: An information system for G protein-coupled receptors. *Nucleic Acids Res* **44**, D356–D364 (2016).

11. Rosenbaum, D. M., Rasmussen, S. G. F. & Kobilka, B. K. The structure and function of G-protein-coupled receptors. *Nature* vol. 459 356–363 Preprint at https://doi.org/10.1038/nature08144 (2009).

12. Zhang, H. *et al.* Structure of the Angiotensin Receptor Revealed by Serial Femtosecond Crystallography Article Structure of the Angiotensin Receptor Revealed by Serial Femtosecond Crystallography. 833–844 (2015) doi:10.1016/j.cell.2015.04.011.

13. Huynh, J., Thomas, W. G., Aguilar, M. I. & Pattenden, L. K. Role of helix 8 in G protein-coupled receptors based on structure-function studies on the type 1 angiotensin receptor. *Mol Cell Endocrinol* **302**, 118–127 (2009).

14. Bonifacino, J. S., Cosson, P. & Klausner, R. D. Colocalized transmembrane determinants for ER degradation and subunit assembly explain the intracellular fate of TCR chains. *Cell* (1990) doi:10.1016/0092-8674(90)90447-M.

15. Tan, P. K., Waites, C., Liu, Y., Krantz, D. E. & Edwards, R. H. A leucine-based motif mediates the endocytosis of vesicular monoamine and acetylcholine transporters. *Journal of Biological Chemistry* (1998) doi:10.1074/jbc.273.28.17351.

16. Neve, K. A., Qanbar, R. & Bouvier, M. Role of palmitoylation/depalmitoylation reactions in G-protein-coupled receptor function. *Pharmacology and Therapeutics* vol. 97 1–33 Preprint at https://doi.org/10.1016/S0163-7258(02)00300-5 (2003).

17. Mostafapour, S., Kobilka, B. K. & von Zastrow, M. Pharmacological sequestration of a chimeric beta 3/beta 2 adrenergic receptor occurs without a corresponding amount of receptor internalization. *Recept Signal Transduct* **6**, 151–163 (1996).

18. Heidorn, D. B. & Trewhell, J. Comparison of the Crystal and Solution Structures of Calmodulin and Troponin C. *Biochemistry* **27**, 909–915 (1988).

19. Introduction to Protein Structure, by Branden, 2nd Edition: Carl Branden,John Tooze: 9788153230505: Amazon.com: Books. https://www.amazon.com/Introduction-Protein-Structure-Branden-2nd/dp/8153230506.

20. Magdeleine, M. *et al.* A filter at the entrance of the Golgi that selects vesicles according to size and bulk lipid composition. *Elife* (2016) doi:10.7554/eLife.16988.

21. Mesmin, B. *et al.* Two lipid-packing sensor motifs contribute to the sensitivity of ArfGAP1 to membrane curvature. *Biochemistry* **46**, 1779–1790 (2007).

22. Høie, M. H. *et al.* NetSurfP-3.0: accurate and fast prediction of protein structural features by protein language models and deep learning. *Nucleic Acids Res* **50**, W510–W515 (2022).

23. Kim, D. I. *et al.* An improved smaller biotin ligase for BioID proximity labeling. *Mol Biol Cell* **27**, 1188–1196 (2016).

24. Kaksonen, M. & Roux, A. Mechanisms of clathrin-mediated endocytosis. *Nat Rev Mol Cell Biol* **19**, 313–326 (2018).

25. Shafaq-Zadah, M., Dransart, E. & Johannes, L. Clathrin-independent endocytosis, retrograde trafficking, and cell polarity. *Current Opinion in Cell Biology* vol. 65 112–121 Preprint at https://doi.org/10.1016/j.ceb.2020.05.009 (2020).

26. Parton, R. G. Caveolae: Structure, Function, and Relationship to Disease. *Annu Rev Cell Dev Biol* **34**, 111–136 (2018).

27. Casamento, A. & Boucrot, E. Molecular mechanism of Fast Endophilin-Mediated Endocytosis. *Biochemical Journal* vol. 477 2327–2345 Preprint at https://doi.org/10.1042/BCJ20190342 (2020).

28. Traub, L. M. Regarding the Amazing Choreography of Clathrin Coats. *PLoS Biol* **9**, e1001037 (2011).

29. Polo, S. *et al.* A single motif responsible for ubiquitin recognition and monoubiquitination in endocytic proteins. *Nature* **416**, 451–455 (2002).

30. Christ, L., Raiborg, C., Wenzel, E. M., Campsteijn, C. & Stenmark, H. Cellular Functions and Molecular Mechanisms of the ESCRT Membrane-Scission Machinery. *Trends in Biochemical Sciences* vol. 42 42–56 Preprint at https://doi.org/10.1016/j.tibs.2016.08.016 (2017).

367 31. Merrifield, C. J., Perrais, D. & Zenisek, D. Coupling between clathrin-coated-pit invagination,
368 cortactin recruitment, and membrane scission observed in live cells. *Cell* **121**, 593–606 (2005).

369 32. Taylor, M. J., Perrais, D. & Merrifield, C. J. A High Precision Survey of the Molecular Dynamics of
370 Mammalian Clathrin-Mediated Endocytosis. *PLoS Biol* **9**, e1000604 (2011).

371 33. Stroh, K. S. & Risselada, H. J. Quantifying Membrane Curvature Sensing of Peripheral Proteins by
372 Simulated Buckling and Umbrella Sampling. *J Chem Theory Comput* **17**, 5276–5286 (2021).

373 34. Dijkman, P. M. *et al.* Conformational dynamics of a G protein–coupled receptor helix 8 in lipid
374 membranes. *Sci Adv* **6**, (2020).

375 35. Schmidt, J. H. *et al.* Constitutive internalization across therapeutically targeted GPCRs correlates
376 with constitutive activity. *Basic Clin Pharmacol Toxicol* **126**, 116–121 (2020).

377 36. Rosenkilde, M. M., Tsutsumi, N., Knerr, J. M., Kildedal, D. F. & Garcia, K. C. Viral G Protein–
378 Coupled Receptors Encoded by β- and γ-Herpesviruses. *https://doi.org/10.1146/annurev-virology-*
379 *100220-113942* **9**, 329–351 (2022).

380 37. Erdogmus, S. *et al.* Helix 8 is the essential structural motif of mechanosensitive GPCRs. *Nat*
381 *Commun* **10**, 1–15 (2019).

382 38. Wang, G. *et al.* The G Protein-Coupled Receptor FFAR2 Promotes Internalization during Influenza
383 A Virus Entry. *J Virol* **94**, (2020).

384 39. Gautier, R., Douguet, D., Antonny, B. & Drin, G. HELIQUEST: a web server to screen sequences
385 with specific -helical properties. *Bioinformatics* **24**, 2101–2102 (2008).

386 40. Jumper, J. *et al.* Highly accurate protein structure prediction with AlphaFold. *Nature* **596**, 583–
387 589 (2021).

Figures and legends

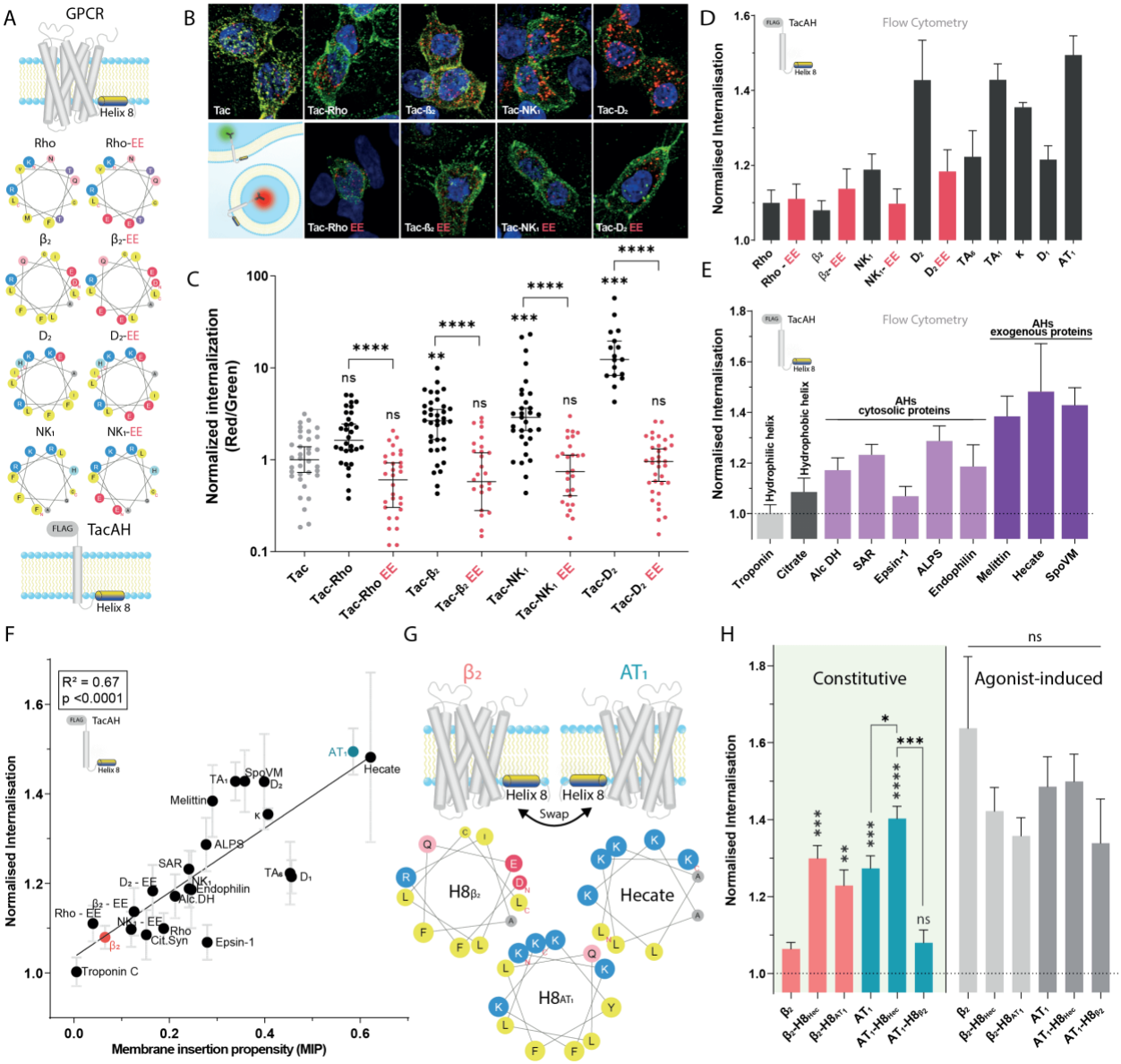

Figure 1. **Amphipathic helices in transmembrane proteins autonomously drive endocytosis**. **a** Illustration of GPCR H8 sequences transferred to the single transmembrane protein Tac for determination of their autonomous endocytic drive alongside mutational disruption of amphipathicity by introduction of negative charges in the hydrophobic face of H8. **b** Representative images of HEK293 cells transfected with Tac-H8 constructs and subjected to antibody feeding (illustrated in insert, lower left). **c** Quantification of internalization (Red/Green

396 fluorescence ratio), relative to Tac, from confocal images (every dot represents a cell, data
397 compiled from three independent experiments). **d** Internalization of Tac-H8 constructs assessed
398 by flow cytometry and normalized to Tac. Mean ± SEM, N=3 **e** Internalization of Tac with AHs
399 from cytosolic proteins or exogenous AHs assessed by flow cytometry. Mean ± SEM, N=3. **f**
400 Linear correlation (R^2 = 0.67 p <0.0001) between Membrane Insertion Propensity (MIP) of Tac-
401 AH constructs and their respective endocytic rate (relative to Tac). Mean ± SEM, N=3. **g**
402 Illustration of chimeric H8 GPCRs with swapped part highlighted in helical wheel
403 representations using HeliQuest [39]. (H) Constitutive and agonist-induced (10 µM agonists; ISO =
404 Isoproterenol and ANGII = angiotensin II) internalization rates of chimeric FLAG-tagged GPCR
405 constructs with swapped H8 sequences relative to Tac. Mean ± SEM, N=3.

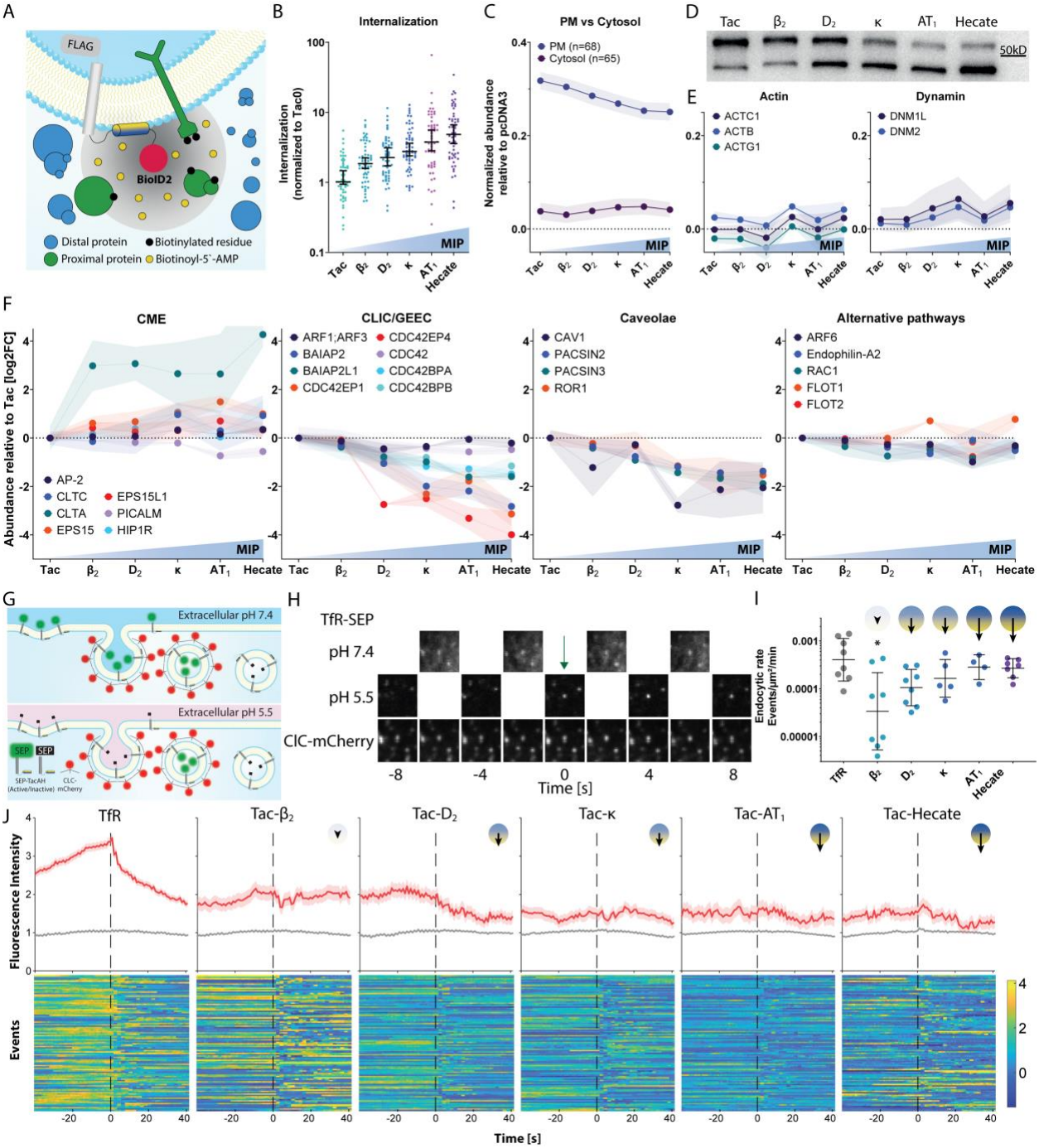

Figure 2. **ToTAM associates with CME machinery in a non-canonical manner. a** Schematic of proximity biotinylation assay with BioID2. **b** Quantification of internalization of Flag-Tac AH BioID2 constructs from confocal images (every dot represents a cell, compiled from three independent experiments). **c** Differences (⍰⍰ in label-free quantification (LFQ) values for

411 indicated constructs versus basal levels (pcDNA) normalized by Tac compiled for all cytosolic and
412 membrane proteins, as defined by a STRING localization score of 5 with no other localization
413 above 4.5. **d** Western blot (M1 ab) of Flag-Tac AH-BioID2 constructs transfected in HEK293 cells
414 showing mature proteins (high MW band) and immature protein (low MW band). **e** Difference
415 in LFQ values versus endogenously biotinylated protein for identified actin and dynamin
416 subunits, respectively. **f** Absolute difference in LFQ values (normalized to Tac) of selected
417 identified proteins associated with CME, CLIG/GEEC, Caveolae and other endocytic pathways. **g**
418 Schematic of (ppH-TIRFM) protocol enabling definition of time of scission for individual
419 endocytic events. **h** Images of representative endocytic event from ppHTIRFM experiments of
420 Super Ecliptic pHluorin (SEP) tagged transferrin receptor (TfR) together with clathrin light chain
421 (CLC)-mCherry. **i** Endocytic event rate for the 5 different SEP-TacAH constructs compared to TfR-
422 SEP. Statistical analysis using Kruskal-Wallis multiple comparisons test. **j** (Upper) Average of
423 individually normalized CLC-mCherry traces for TfR-SEP and 5 SEP-TacAH constructs. (Lower)
424 Heatmaps of normalized individual CLC-mCherry traces pre- and post-scission. N = 5-10 cells
425 (846-2797 events) per condition.

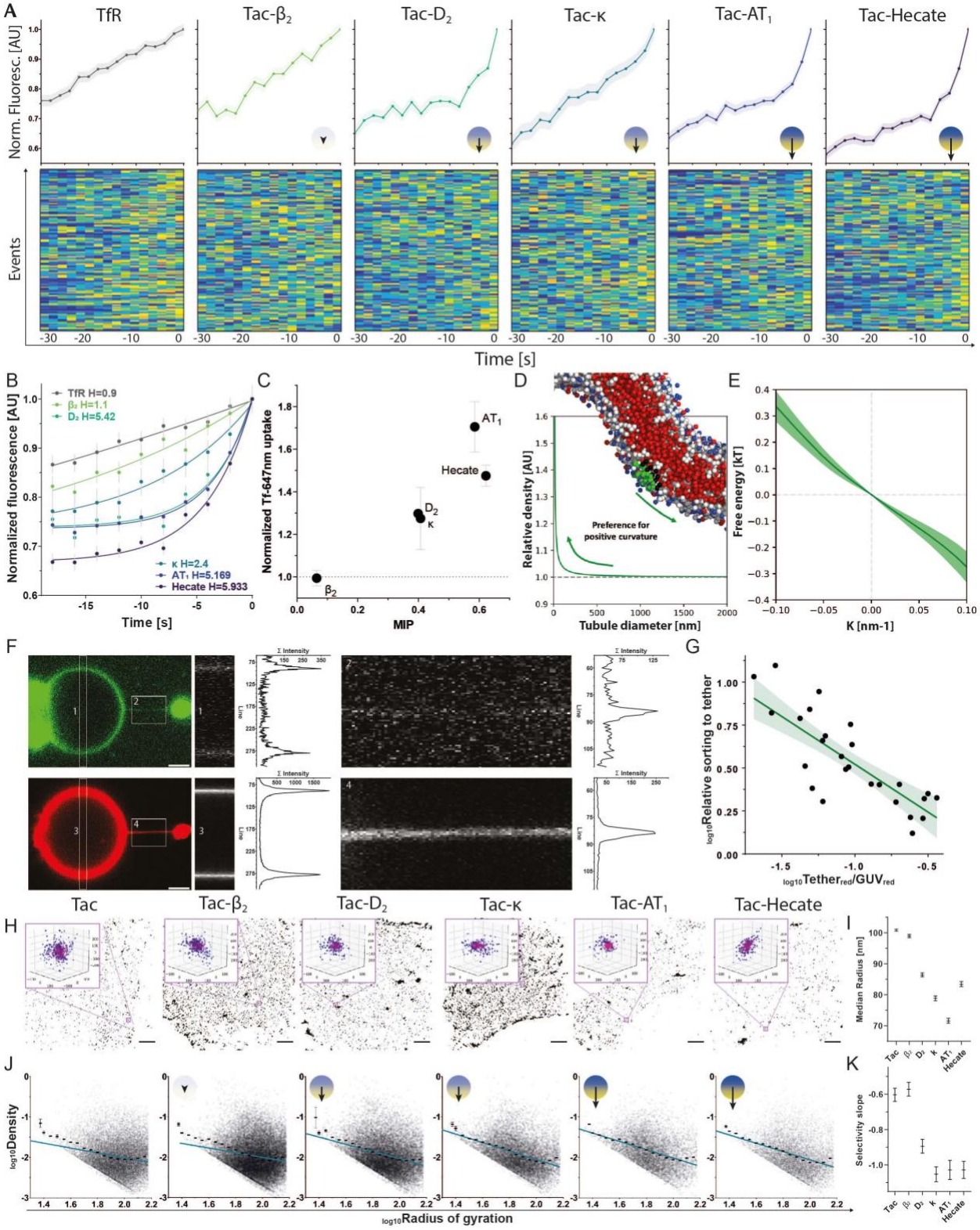

Figure 3. **Amphipathic helices in transmembrane proteins promote endocytosis through association with curved membranes. a** (Upper) Average of individually normalized pH 7.4 TfR-

429 SEP and SEP-TacAH fluorescence intensity traces building up to point of scission (Time = 0).
430 (Lower) Heatmaps of normalized individual SEP-fluorescence profiles at pH 7.4 of TfR-SEP and
431 SEP-TacAH constructs prior to scission. N = 5-10 cells per condition, n = 518-2367 total traces. **b**
432 Non-linear regression fits of averaged normalized pHluorin traces up to point of scission. H is
433 the Hill coefficient. **c** Effect of TacAH constructs on AF647-labelled transferrin endocytosis in
434 trans, by flow cytometry. **d** Relative protein density (Hecate peptide) as a function of tubule
435 diameter determined in buckled membrane MD analysis indicating a strong preference for
436 positive curvature. **e** Free energy from (**d**) as a function of membrane curvature. **f** Tethers pulled
437 from GUVs (red) pre-incubated with Oregon Green labelled Hecate peptide (green). Insert 1 and
438 3, zooms of GUV and summed intensity profile. Insert 2 and 4, zooms of tether and summed
439 intensity profile. **g** Quantification of the relative sorting to the tether as a function of relative
440 size of the tether (Tetherred/GUVred). **h** Representative 3D-dSTORM images of FLAG-Tac and 5
441 FLAG-TacAH constructs after surface labelling with Alexa Fluor 647-conjugated aFLAG antibody,
442 scale bar 5 µm. Inserts show representative single clusters. **i** Average size of clusters for the
443 individual constructs, median ± 95% CI, N=6. **j** Logarithmic relationship of cluster size and cargo
444 density (FLAG-Tac-AH). Black bars show binned averages ± SEM and the blue line represents a
445 linear fit of the data. Better adherence of the fit to the binned averages indicates curvature
446 dependent sorting for Tac-AH constructs with high MIP **k** Selectivity slope (i.e., curvature
447 sensitivity) derived for linear fits with error on log-log plots of the data in (**j**) (see Figure S16).
448

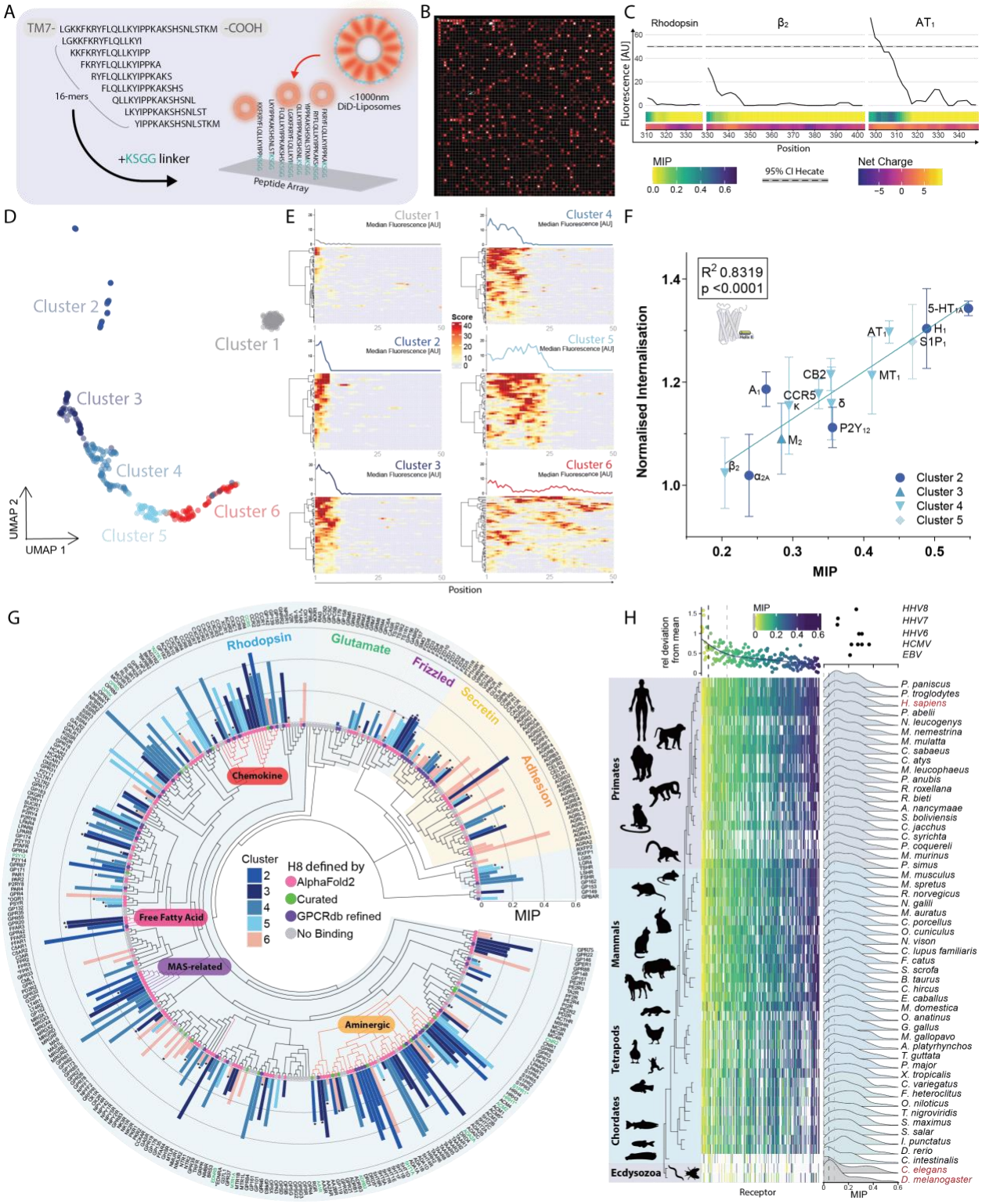
A
TM7- LGKKFKRYFLQLLKYIPPKAKSHSNLSTKM -COOH
16-mers
+KSGG linker
<1000nm DiD-Liposomes
Peptide Array
B
C
Rhodopsin
β2
AT1
Fluorescence [AU]
Position
MIP
95% CI Hecate
Net Charge
D
Cluster 1
Cluster 2
Cluster 3
Cluster 4
Cluster 5
Cluster 6
UMAP 1
UMAP 2
E
Median Fluorescence [AU]
Score
Position
F
R2 0.8319
p <0.0001
Normalised Internalisation
MIP
5-HT1A
H1
S1P1
AT1
MT1
CB2
A1
CCR5
κ
δ
P2Y12
M2
β2
α2A
G
Rhodopsin
Glutamate
Frizzled
Secretin
Adhesion
Chemokine
Free Fatty Acid
MAS-related
Aminergic
Cluster
2
3
4
5
6
H8 defined by
AlphaFold2
Curated
GPCRdb refined
No Binding
MIP
H
rel deviation from mean
MIP
HHV8
HHV7
HHV6
HCMV
EBV
Primates
Mammals
Tetrapods
Chordates
Ecdysozoa
P. paniscus
P. troglodytes
H. sapiens
P. abelii
N. leucogenys
M. nemestrina
M. mulatta
C. sabaeus
C. atys
M. leucophaeus
P. anubis
R. roxellana
R. bieti
A. nancymaae
S. boliviensis
C. jacchus
C. syrichta
P. coquereli
M. murinus
P. simus
M. musculus
M. spretus
R. norvegicus
N. galili
M. auratus
C. porcellus
O. cuniculus
N. vison
C. lupus familiaris
F. catus
S. scrofa
B. taurus
C. hircus
E. caballus
M. domestica
O. anatinus
G. gallus
M. gallopavo
A. platyrhynchos
T. guttata
P. major
X. tropicalis
C. variegatus
F. heteroclitus
O. niloticus
T. nigroviridis
S. maximus
S. salar
I. punctatus
D. rerio
C. intestinalis
C. elegans
D. melanogaster
Receptor
MIP

449

450 Figure 4. **Proteome-wide characterization of C-terminal membrane interactions in GPCRs and**
451 **their role in constitutive endocytosis of therapeutically relevant GPCRs. a** Schematic of chip
452 array for scanning of liposome binding strength throughout the full range of human GPCR C-
453 termini at dual AA resolution. Individual peptides are randomly positioned on the chip. **b**
454 Representative image of fluorescent signal from bound liposomes on zoomed in area of array.
455 Regular pattern in top left corner is control Hecate peptide. **c** Compiled binding profile of the C-
456 termini of Rhodopsin, β2AR and ATR along with corresponding MIP and net charge values
457 displayed below. **d** UMAP-based clustering of all human GPCR C-termini based on position and
458 strength of liposome binding. **e** Heatmaps of all individual GPCR C-terminal liposome binding
459 profiles within the six clusters and profile plots of the median fluorescence intensity (line above)
460 (see S19 from detailed view). **f** Linear correlation ($R^2 = 0.83$, $p < 0.0001$) between MIP of H8 from
461 clusters 2-5, based on sequences (Figure S20) in most pharmacologically relevant GPCRs and
462 their respective endocytic rate (relative to Tac) determined by flow cytometry [35]. Mean ± SEM,
463 N=3. **g** Circular phylogenetic tree of human GPCRs based on sequence homology and divided
464 into GRAFS families and clusters, alongside the corresponding calculated MIP based on H8 from
465 either refined representative structures as annotated on GPCRdb (purple) [10], AlphaFold2
466 prediction (magenta) [40]. Receptors used in (**f**) are highlighted by green and receptors described
467 as mechanosensitive [37] are highlighted by asterisks (name). GPCRs from cluster 1 (no binding) in
468 grey. Receptors with a structural H8 predicted longer than 20 amino acids marked with asterisk
469 (bar). **h** Evolutionary tree of GPCRs displaying MIP of H8 sequences identified in Human
470 receptors and aligned across species (left). The ratio of variance vs. mean of all MIP decrease

471 with increasing MIP (upper, left). (Upper, right) MIP values for viral GPCRs (Table S2). (Lower

472 right) Density distribution of MIP values for individual species shift to the right during evolution.

473